

Exact 3-D Channel Impulse Response Under Uniform Drift for Absorbing Spherical Receivers

Yen-Chi Lee, *Member, IEEE*, Ping-Cheng Yeh, *Member, IEEE*, and Chia-Han Lee, *Member, IEEE*

arXiv:2512.04858v2 [cs.IT] 4 Feb 2026

Abstract—An exact channel impulse response (CIR) for the three-dimensional point-to-sphere absorbing channel under drift has remained unavailable due to symmetry breaking. This letter closes this gap by deriving an exact analytical CIR for a fully absorbing spherical receiver under uniform drift with arbitrary direction. By formulating the problem in terms of joint first-hitting time–location statistics and applying a Girsanov-based measure change, drift effects are isolated into an explicit multiplicative factor, yielding an exact series representation. The resulting CIR provides a rigorous reference model and enables efficient, noise-free evaluation of key channel metrics without relying on Monte Carlo simulations.

Index Terms—Molecular communication via diffusion (MCvD), channel modeling, channel impulse response (CIR), first-hitting statistics, stochastic differential equations (SDE).

I. INTRODUCTION

FOR three-dimensional molecular communication (MC) systems [1]–[3], the point-to-sphere absorbing channel has long served as a canonical reference model [4]. Its analytical tractability, however, relies critically on strong geometric symmetries that are immediately broken once drift is introduced.

In practical MC environments, drift is not a secondary effect but a fundamental transport mechanism, arising from background flow [5], [6], externally induced bias fields [7], [8], or spatial concentration gradients. Even when the drift field is spatially uniform, its presence breaks the radial symmetry that underlies classical no-drift formulations [9]. As a result, the first-hitting statistics depend not only on the arrival time but also on the angular location at which particles are absorbed.

Despite its physical relevance, an exact channel impulse response (CIR) for the point-to-sphere geometry under arbitrary drift direction has remained unavailable. Existing analytical results are restricted to zero-drift scenarios [9], aligned drift configurations [10], or reduced-dimensional approximations [5], [6], while more general settings are typically handled through Monte Carlo simulations or empirical fitting [4], [11]. This lack of an exact reference model has limited both physical interpretability and systematic channel analysis in drift-dominated regimes.

This work was supported by the National Science and Technology Council of Taiwan (NSTC 113-2115-M-008-013-MY3). (Corresponding author: Yen-Chi Lee.)

Y.-C. Lee is with the Department of Mathematics, National Central University, Taoyuan, Taiwan (e-mail: ycllee@math.ncu.edu.tw).

P.-C. Yeh is with the Graduate Institute of Communication Engineering, National Taiwan University, Taipei, Taiwan (e-mail: pcyeh@ntu.edu.tw).

C.-H. Lee is with the Institute of Communications Engineering, National Yang Ming Chiao Tung University, Hsinchu, Taiwan (e-mail: chiahan@nycu.edu.tw).

In this letter, we close this gap by deriving an exact analytical CIR for an absorbing spherical receiver¹ in 3-D space under uniform drift with arbitrary direction. Rather than modifying existing no-drift expressions, we formulate the problem at the level of the *joint* first-hitting time and location statistics. By applying a measure-change argument based on the Girsanov theorem [12], the effect of drift is incorporated as an explicit reweighting of boundary hitting events, while preserving the analytical structure of the baseline no-drift solution.

The resulting CIR admits an exact series representation that remains valid for arbitrary drift orientations and strengths. This formulation provides a rigorous reference model for drifted point-to-sphere channels, resolving a long-standing symmetry-breaking regime that has previously been treated only approximately or through simulation [4], [13]–[15]. Beyond channel characterization, the availability of an exact CIR enables efficient and noise-free extraction of key system metrics, such as peak time and peak amplitude [9], [16], which are difficult to obtain reliably from particle-based Monte Carlo methods.

The main contributions of this letter are summarized as follows:

- An exact analytical series expression (6) for the 3-D point-to-sphere CIR under uniform drift with arbitrary direction.
- A measure-change-based framework (see Fig. 2), via the Girsanov theorem, that isolates drift effects into an explicit multiplicative factor and admits extension to other molecular channel models.

TABLE I: Comparison of related analytical CIR results in MC literature. Note that in 1-D space, spherical and planar geometries coincide as the receiver reduces to a point boundary.

Dim.	No Drift	Uniform Drift
$d = 1$	Lévy distribution [5], [6]	Inverse Gaussian distribution [5], [6]
$d = 3$ (Planar)	Exact analytical CIR [17]	Exact analytical CIR (arbitrary direction) [17]
$d = 3$ (Spherical)	Exact analytical CIR [9]	No exact analytical CIR in prior work; [10] restricted to aligned drift

II. SYSTEM MODEL

We consider an unbounded 3-D fluid environment \mathbb{R}^3 . The transmitter (Tx) is modeled as a point source located at $\mathbf{x}_0 \in$

¹In the molecular communication literature, a fully absorbing spherical receiver is widely used as a standard model for ligand–receptor binding or perfect capture at the receiver surface.

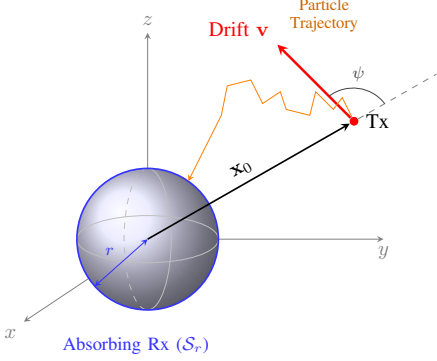


Fig. 1: System model of the 3-D molecular communication channel. A point transmitter is located at \mathbf{x}_0 , and a fully absorbing spherical receiver of radius r is at the origin. The medium is subject to a uniform drift \mathbf{v} forming an angle $\psi = \angle(\mathbf{v}, \mathbf{x}_0)$.

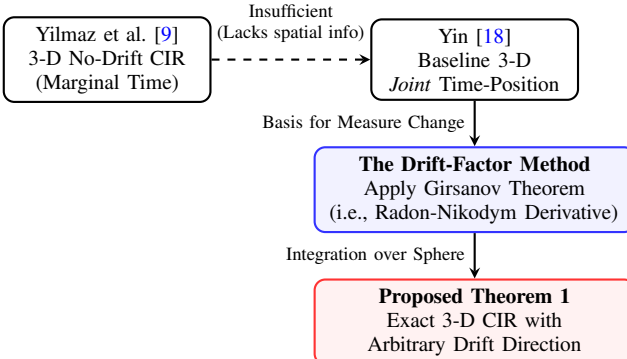


Fig. 2: Derivation flow based on drift-factor method. We start from Yin's joint time-position distribution [18] and apply the Girsanov theorem to derive the 3D CIR in analytical form.

\mathbb{R}^3 , and the receiver (Rx) is a fully absorbing sphere of radius r centered at the origin, denoted by \mathcal{S}_r , with $|\mathbf{x}_0| > r$. The system geometry is illustrated in Fig. 1.

Information particles (molecules) are released at time $t = 0$. From a microscopic perspective, the trajectory of a particle \mathbf{X} follows the Itô stochastic differential equation [12]

$$d\mathbf{X}_t = \mathbf{u}(t) dt + \sigma d\mathbf{B}_t, \quad \mathbf{X}_0 = \mathbf{x}_0, \quad (1)$$

where \mathbf{B}_t is a standard 3-D Brownian motion, D is the diffusion coefficient, and $\sigma = \sqrt{2D}$.

While the proposed framework applies to general drift profiles, this letter focuses on the practically relevant case of *constant uniform drift*, $\mathbf{u}(t) \equiv \mathbf{v} \in \mathbb{R}^3$, forming an angle $\psi = \angle(\mathbf{v}, \mathbf{x}_0)$ with the Tx-Rx axis. The relative strength of advection and diffusion is characterized by the Péclet number $\text{Pe} = |\mathbf{v}|r/D$. The first hitting time is defined as $T \triangleq \inf\{t > 0 : |\mathbf{X}_t| = r\}$, and the CIR is the probability density function of T , denoted by $f_{3D}^{(\mathbf{v})}(t)$.

From a macroscopic viewpoint, the corresponding particle concentration satisfies the advection-diffusion equation with absorbing boundary conditions. However, for arbitrary drift directions, direct PDE-based approaches become analytically intractable, which motivates the stochastic measure-change formulation adopted in the next section.

III. DERIVATION OF THE DRIFTED 3-D CIR

This section derives the exact CIR for a spherical absorbing receiver in 3-D space under a uniform drift with arbitrary direction. The overall derivation flow is summarized in Fig. 2. The key idea is to bridge the well-established no-drift case and the general drifted case through a measure-change argument.

A. Motivation: Why the Joint Distribution Is Necessary

Existing analytical results for spherical receivers without drift typically rely on the marginal first-hitting-time distribution [9]. However, under drift, advection introduces a strong directional bias: the contribution of each hitting event depends not only on *when* the particle hits the receiver, but also on *where* it hits the spherical boundary. Consequently, the marginal hitting-time distribution alone is insufficient to characterize the drifted CIR.

To retain this spatial information, we start from the joint probability density of the first hitting time T and the hitting location \mathbf{X}_T on the spherical boundary \mathcal{S}_r , denoted by $f_{3D}^{(0)}(t, \mathbf{y})$ for $\mathbf{y} \in \mathcal{S}_r$. An explicit analytical expression for this joint density in the no-drift case is available from probability literature [18] and serves as the baseline of our derivation.

B. Drift-Factor Representation via Girsanov Theorem

To incorporate drift, we employ the Girsanov theorem [12] to perform a change of measure from a reference no-drift process (measure \mathbb{Q}) to the drifted process (measure \mathbb{P}). Evaluated at the hitting time, this change of measure introduces a multiplicative *drift factor*, which analytically relates the drifted joint density to the no-drift one through

$$f_{3D}^{(\mathbf{v})}(t, \mathbf{y}) = \exp\left(\frac{\mathbf{v} \cdot (\mathbf{y} - \mathbf{x}_0)}{\sigma^2} - \frac{|\mathbf{v}|^2 t}{2\sigma^2}\right) f_{3D}^{(0)}(t, \mathbf{y}). \quad (2)$$

Physically, the drift factor reweights each hitting event according to the work done by the drift along the particle trajectory. Hitting locations aligned with the drift direction are exponentially favored, while those against the drift are suppressed. This representation isolates the effect of drift into a single, explicit weighting term (the drift factor) while preserving the analytical structure of the no-drift joint distribution.

C. Baseline Joint Density for the No-Drift Case

For a Tx located outside the spherical Rx (i.e., $|\mathbf{x}_0| > r$), the joint density of the hitting time-location for a 3-D Brownian motion without drift admits the following series representation, adapted from [18, Theorem 3.2]:

$$f_{3D}^{(0)}(t, \mathbf{y}) = \frac{1}{2\pi} \frac{r}{|\mathbf{x}_0|} \sum_{m=0}^{\infty} \left(m + \frac{1}{2}\right) P_m(\cos \angle(\mathbf{x}_0, \mathbf{y})) \times \int_0^{\infty} \frac{\lambda Z_{m+\frac{1}{2}}(|\mathbf{x}_0|/r, \lambda r/\sigma)}{J_{m+\frac{1}{2}}^2(\lambda r/\sigma) + Y_{m+\frac{1}{2}}^2(\lambda r/\sigma)} \exp(-\frac{1}{2}\lambda^2 t) d\lambda. \quad (3)$$

where $P_m(\cdot)$ denotes the Legendre polynomial and $Z_{\nu}(a, b) = J_{\nu}(ab)Y_{\nu}(b) - J_{\nu}(b)Y_{\nu}(ab)$ denotes the standard cross-product of Bessel functions under normalized radial coordinates.

D. CIR as Surface Marginalization

The drifted CIR is defined as the marginal distribution of the random hitting time T , obtained by integrating the drifted joint density over the spherical boundary:

$$f_{3D}^{(\mathbf{v})}(t) = \int_{\mathcal{S}_r} f_{3D}^{(\mathbf{v})}(t, \mathbf{y}) ds(\mathbf{y}). \quad (4)$$

Substituting (2) into (4), the \mathbf{y} -independent term $\exp(-|\mathbf{v}|^2 t / 2\sigma^2 - \mathbf{v} \cdot \mathbf{x}_0 / \sigma^2)$ can be factored out. The remaining task is to evaluate surface integrals of the form $e^{\mathbf{v} \cdot \mathbf{y} / \sigma^2}$ multiplied by the angular modes in (3).

E. Mode-Wise Surface Integration

To evaluate these integrals, we adapt the following identity from [18, Lemma 2.5] specialized to the 3-D setting.

Lemma 1 (3-D Surface Integral Identity). *For any vector $\mathbf{c} \in \mathbb{R}^3$,*

$$\begin{aligned} & \int_{\mathcal{S}_r} e^{\mathbf{c} \cdot \mathbf{y}} P_m(\cos \angle(\mathbf{x}_0, \mathbf{y})) ds(\mathbf{y}) \\ &= 2(r\pi)^{\frac{3}{2}} \left(\frac{|\mathbf{c}|}{2} \right)^{-\frac{1}{2}} I_{m+\frac{1}{2}}(|\mathbf{c}|r) P_m(\cos \angle(\mathbf{c}, \mathbf{x}_0)), \end{aligned} \quad (5)$$

where $I_\nu(\cdot)$ denotes the modified Bessel function of the first kind.

Applying Lemma 1 with $\mathbf{c} = \mathbf{v}/\sigma^2$, the angular argument reduces to $\angle(\mathbf{v}, \mathbf{x}_0) = \psi$. Substituting (3) into (4), the CIR decomposes into a summation over angular eigenmodes m , where each term involves a single surface integral that can be evaluated explicitly using Lemma 1. Collecting all prefactors yields the exact 3-D CIR stated below in Theorem 1.

Theorem 1 (Exact 3-D CIR under uniform drift). *In \mathbb{R}^3 , the CIR for a spherical absorbing receiver of radius r under a uniform drift \mathbf{v} is*

$$\begin{aligned} f_{3D}^{(\mathbf{v})}(t) &= -\exp\left(-\frac{\mathbf{v} \cdot \mathbf{x}_0}{\sigma^2} - \frac{|\mathbf{v}|^2 t}{2\sigma^2}\right) \frac{\sqrt{2}\sigma}{\sqrt{\pi}|\mathbf{v}|^{1/2}|\mathbf{x}_0|^{1/2}} \\ &\times \sum_{m=0}^{\infty} \left(m + \frac{1}{2}\right) I_{m+\frac{1}{2}}\left(\frac{|\mathbf{v}|r}{\sigma^2}\right) P_m(\cos \psi) \\ &\times \int_0^{\infty} \frac{\lambda Z_{m+\frac{1}{2}}(|\mathbf{x}_0|/r, \lambda r/\sigma)}{J_{m+\frac{1}{2}}^2(\lambda r/\sigma) + Y_{m+\frac{1}{2}}^2(\lambda r/\sigma)} e^{-\frac{1}{2}\lambda^2 t} d\lambda, \end{aligned} \quad (6)$$

where $\psi = \angle(\mathbf{v}, \mathbf{x}_0)$, $\sigma^2 = 2D$, $I_\nu(\cdot)$ is the modified Bessel function of the first kind, and $P_m(\cdot)$ is the Legendre polynomial.

This exact representation (6) serves as the basis for the numerical evaluation and performance characterization presented in the next section.

IV. NUMERICAL RESULTS AND DISCUSSION

In this section, we validate the derived exact analytical CIR against particle-based Monte Carlo simulations and give a brief discussion on how the proposed formulation enables

efficient characterization of two key channel metrics: pulse amplitude and pulse peak time. All numerical evaluations and simulations are performed using MATLAB (MathWorks cloud-based environment). To ensure consistency with established MCvD channel modeling literature [9], the default system parameters are chosen typically as follows: diffusion coefficient $D = 80 \mu\text{m}^2/\text{s}$, receiver radius $r = 10 \mu\text{m}$, and initial distance $|\mathbf{x}_0| = 20 \mu\text{m}$. We consider two representative drift scenarios: a moderate drift speed ($|\mathbf{v}| = 5 \mu\text{m/s}$) and a higher drift speed ($|\mathbf{v}| = 10 \mu\text{m/s}$).

For Monte Carlo validation shown in Fig. 3, the analytical CIR is discretized over a fixed time bin Δt to enable a direct comparison with particle-based simulations. In Figs. 4 and 5, the peak time t_{peak} is obtained by maximizing the continuous-time analytical CIR, while the corresponding peak amplitude is reported in terms of the expected number of absorbed molecules per time bin, $N_{\text{tx}} f_{3D}^{(\mathbf{v})}(t_{\text{peak}}) \Delta t$, using the same Δt as in Fig. 3 for consistent scaling.

A. Validation against Monte Carlo Simulations

Fig. 3 compares the analytical CIR (Eq. (6), truncated at $m = 30$) with particle-based Monte Carlo simulations using $N_{\text{tx}} = 10^6$ molecules, for drift magnitudes $|\mathbf{v}| \in \{5, 10\} \mu\text{m/s}$ and drift angles $\psi \in \{0^\circ, 90^\circ, 180^\circ\}$. Excellent agreement is observed across all considered scenarios.

As shown in Fig. 3, increasing drift aligned with the Tx–Rx axis sharpens the received pulse, whereas drift directed away from the receiver suppresses the peak and elongates the tail. These trends are accurately captured by the analytical CIR. Any residual discrepancies are attributable to finite-particle fluctuations inherent in Monte Carlo simulations.

B. Convergence of the Analytical Series

Numerical evaluation of Theorem 1 requires truncation of the infinite series over the angular mode index m . From the structure of (6), the truncation order M controls the angular resolution of the CIR through the Legendre modes $P_m(\cos \psi)$, while temporal smoothing is governed by the Gaussian factor $e^{-\lambda^2 t/2}$ in the radial integral.

For moderate drift strengths, higher-order angular modes are increasingly suppressed by the modified Bessel term $I_{m+\frac{1}{2}}(|\mathbf{v}|r/\sigma^2)$, and truncation at $M = 30$ yields a relative error below 10^{-5} over most of the time domain for the parameters considered in this work. This accuracy is sufficient for Monte Carlo validation and for the extraction of peak metrics.

Convergence becomes slower only in the immediate vicinity of the first arrival (very small t), where temporal smoothing is weak and sharper angular features must be resolved, or under stronger drift conditions that induce pronounced angular anisotropy. In such cases, increasing the truncation order to $M \approx 50$ provides accurate resolution of the initial transient. For practical operating regimes, $M = 30$ offers an effective accuracy–complexity trade-off.

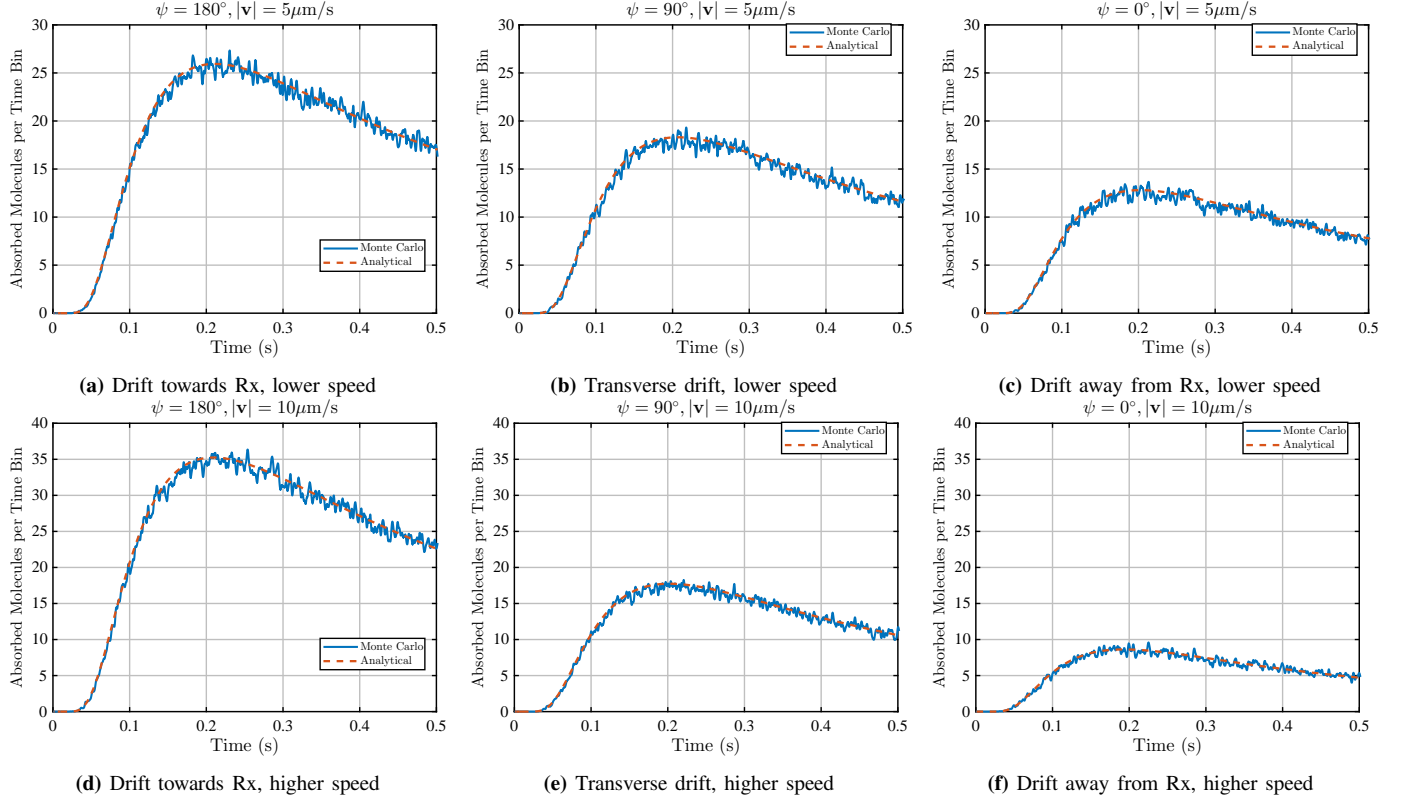


Fig. 3: Validation of analytical CIR against Monte Carlo simulations. The analytical curves correspond to $N_{tx}f_{3D}^{(v)}(t)\Delta t$, i.e., the expected number of absorbed molecules within a fixed time bin $\Delta t = 5 \times 10^{-5}$ s. **Top Row:** Moderate drift speed ($|v| = 5 \mu\text{m}/\text{s}$). **Bottom Row:** Higher drift speed ($|v| = 10 \mu\text{m}/\text{s}$). Columns correspond to positive ($\psi = 180^\circ$), transverse ($\psi = 90^\circ$), and negative ($\psi = 0^\circ$) drift directions.

C. Characterization of Peak Metrics

Monte Carlo estimation of peak metrics is computationally expensive because extensive averaging is needed to suppress stochastic fluctuations. In contrast, the analytical CIR provides a smooth objective function, enabling efficient numerical maximization. Compared with particle-based Monte Carlo estimation, this approach reduces the computational cost by several orders of magnitude, as it avoids repeated stochastic sampling and averaging.

Fig. 4 reports peak metrics versus drift magnitude. The peak absorption count is reported as the expected number of absorbed molecules within a fixed time bin Δt , whereas t_{peak} is obtained directly from the continuous-time analytical CIR. As $|v|$ increases, the peak count grows under positive drift and is strongly suppressed under negative drift, while t_{peak} decreases monotonically.

The trends observed in Fig. 5 arise from the underlying geometry of the absorbing receiver rather than from normalization or parameter choices. Increasing the receiver radius enlarges the absorbing surface, thereby enhancing the instantaneous capture probability and leading to a higher peak absorption count. At the same time, a larger radius reduces the effective propagation distance $|\mathbf{x}_0| - r$, which naturally advances the peak time.

V. CONCLUSION

This letter establishes an exact analytical characterization of the 3-D CIR for MCvD systems with a fully absorbing

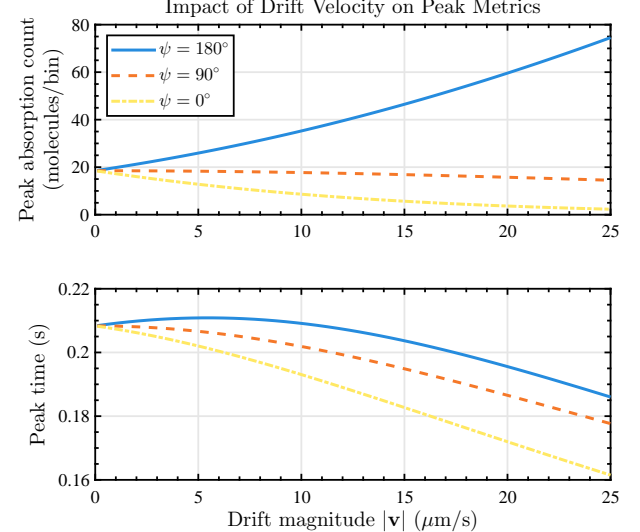


Fig. 4: Impact of drift magnitude $|v|$ on peak metrics for a fixed receiver radius $r = 10 \mu\text{m}$. **Top:** peak absorption count per time bin, computed as $N_{tx}f_{3D}^{(v)}(t_{\text{peak}})\Delta t$ with $\Delta t = 5 \times 10^{-5}$ s (same bin width as in Fig. 3 for consistent scaling). **Bottom:** corresponding peak time t_{peak} , obtained by maximizing the continuous-time analytical CIR and thus independent of Δt . Positive ($\psi = 180^\circ$), transverse ($\psi = 90^\circ$), and negative ($\psi = 0^\circ$) drift directions are shown.

spherical receiver under uniform drift of arbitrary direction. By formulating the problem at the level of joint first-hitting time and location statistics and applying a measure-change

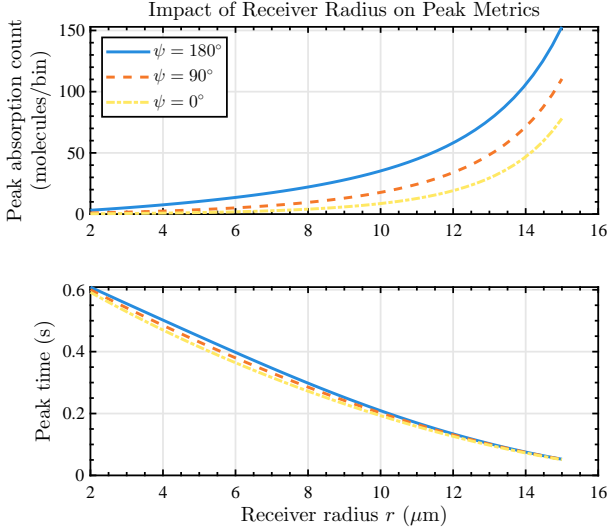


Fig. 5: Impact of receiver radius r on peak metrics for a fixed drift magnitude $|\mathbf{v}| = 10 \mu\text{m/s}$. **Top:** peak absorption count per time bin, computed as $N_{\text{tx},3\text{D}} f_{3\text{D}}^{(\mathbf{v})}(t_{\text{peak}}) \Delta t$ with $\Delta t = 5 \times 10^{-5} \text{ s}$ (same bin width as in Fig. 3 for consistent scaling). **Bottom:** corresponding peak time t_{peak} , obtained by maximizing the continuous-time analytical CIR and thus independent of Δt . Positive ($\psi = 180^\circ$), transverse ($\psi = 90^\circ$), and negative ($\psi = 0^\circ$) drift directions are shown.

argument, we derive an exact series representation of the CIR within the drift-diffusion model, without relying on geometric approximations [10] or dimensional reductions [6]. The analytical CIR is validated against particle-based Monte Carlo simulations over representative drift magnitudes and orientations, showing excellent agreement. Beyond validation, the exact formulation enables efficient and noise-free extraction of key channel metrics via direct numerical maximization with respect to the CIR curve with substantially lower computational cost than simulation-based approaches. Numerical results further clarify how drift orientation and receiver geometry jointly shape the received signal, capturing enhancement, suppression, and geometric scaling effects in a unified manner. From a system-level perspective, the proposed CIR provides a precise and computationally tractable channel model that can be potentially integrated into molecular MIMO detection and receiver design (e.g., [11], [15]), completing a previously missing exact reference model for drifted point-to-sphere molecular channels [4].

APPENDIX A METHODOLOGICAL CONSISTENCY CHECK

This appendix provides a brief *consistency check* for the proposed measure-change framework. It is *not* used as a reduction or a derivation step for the 3-D spherical model in the main text.

In one dimension, an absorbing boundary implies a deterministic point hitting location on the hitting event. Let the initial distance be $\ell > 0$ and $\sigma^2 = 2D$. The no-drift first-hitting-time density is $f_{1\text{D}}^{(0)}(t) = \frac{\ell}{\sqrt{4\pi Dt^3}} \exp\left(-\frac{\ell^2}{4Dt}\right)$, $t > 0$, see [5]. Under constant drift v (towards the boundary), the Girsanov factor evaluated at the hitting time reduces to $\exp\left(\frac{v\ell}{2D} - \frac{v^2 t}{4D}\right)$,

corresponding to (2) with $\mathbf{v} \cdot (\mathbf{y} - \mathbf{x}_0) = v\ell$ in one dimension. Multiplying this factor with the no-drift density $f_{1\text{D}}^{(0)}(t)$ yields

$$f_{1\text{D}}^{(v)}(t) = \frac{\ell}{\sqrt{4\pi Dt^3}} \exp\left(-\frac{\ell^2}{4Dt} + \frac{v\ell}{2D} - \frac{v^2 t}{4D}\right) \\ = \frac{\ell}{\sqrt{4\pi Dt^3}} \exp\left(-\frac{(\ell - vt)^2}{4Dt}\right), \quad (7)$$

where the exponent is obtained by completing the square. This recovers the standard inverse Gaussian first-passage-time law (cf. [5], [6]), which corresponds to the 1-D uniform-drift case as presented in Table I.

REFERENCES

- [1] I. F. Akyildiz, F. Brunetti, and C. Blázquez, “Nanoneetworks: A new communication paradigm,” *Computer Networks*, vol. 52, no. 12, pp. 2260–2279, 2008.
- [2] T. Nakano, A. Eckford, and T. Haraguchi, *Molecular Communication*. Cambridge University Press, 2013.
- [3] N. Farsad, H. B. Yilmaz, A. Eckford, C.-B. Chae, and W. Guo, “A comprehensive survey of recent advancements in molecular communication,” *IEEE Communications Surveys & Tutorials*, vol. 18, no. 3, pp. 1887–1919, 2016.
- [4] V. Jamali, A. Ahmadzadeh, W. Wicke, A. Noel, and R. Schober, “Channel modeling for diffusive molecular communication—a tutorial review,” *Proceedings of the IEEE*, vol. 107, no. 7, pp. 1256–1301, 2019.
- [5] K. V. Srinivas, A. W. Eckford, and R. S. Adve, “Molecular communication in fluid media: The additive inverse Gaussian noise channel,” *IEEE Transactions on Information Theory*, vol. 58, no. 7, pp. 4678–4692, 2012.
- [6] S. Kadloor, R. S. Adve, and A. W. Eckford, “Molecular communication using Brownian motion with drift,” *IEEE Transactions on NanoBioscience*, vol. 11, no. 2, pp. 89–99, 2012.
- [7] Z. Ma, M. Liu, H. Yan, and L. Lin, “Electric field assisted molecular communication for high data rate transmission,” *IEEE Wireless Communications Letters*, vol. 8, no. 6, pp. 1571–1574, 2019.
- [8] P.-C. Chou, Y.-F. Lo, C.-H. Lee, and P.-C. Yeh, “Molecular communications enhanced by time-varying electric field,” *IEEE Transactions on NanoBioscience*, vol. 21, no. 2, pp. 301–311, 2021.
- [9] H. B. Yilmaz, A. C. Heren, T. Tugcu, and C.-B. Chae, “Three-dimensional channel characteristics for molecular communications with an absorbing receiver,” *IEEE Communications Letters*, vol. 18, no. 6, pp. 929–932, 2014.
- [10] B. C. Akdeniz, H. B. Yilmaz, A. E. Pusane, and T. Tugcu, “Impulse response of 3-D molecular communication,” in *Proceedings of the 3rd Workshop on Molecular Communications*, Ghent, Belgium, Apr. 2018.
- [11] M. Ahuja and M. R. Bhatnagar, “Performance analysis and receiver design of spatio-temporal coded modulation scheme for diffusion-based molecular MIMO systems,” *IEEE Transactions on Molecular, Biological and Multi-Scale Communications*, vol. 8, no. 3, pp. 119–137, Sep. 2022.
- [12] B. Øksendal, *Stochastic Differential Equations: An Introduction with Applications*, 6th ed. Springer, 2003.
- [13] A. Noel, K. C. Cheung, and R. Schober, “Optimal receiver design for diffusive molecular communication with flow and additive noise,” *IEEE transactions on nanobioscience*, vol. 13, no. 3, pp. 350–362, 2014.
- [14] B.-H. Koo, C. Lee, H. B. Yilmaz, N. Farsad, A. W. Eckford, and C.-B. Chae, “Molecular MIMO: From theory to prototype,” *IEEE Journal on Selected Areas in Communications*, vol. 34, no. 3, pp. 600–614, 2016.
- [15] M. C. Gursoy, E. Basar, A. E. Pusane, and T. Tugcu, “Index modulation for molecular communication via diffusion systems,” *IEEE Transactions on Communications*, vol. 67, no. 5, pp. 3337–3350, 2019.
- [16] B. Tepekule, A. E. Pusane, H. B. Yilmaz, C.-B. Chae, and T. Tugcu, “ISI mitigation techniques in molecular communication,” *IEEE Transactions on Molecular, Biological, and Multi-Scale Communications*, vol. 1, no. 2, pp. 202–216, 2015.
- [17] Y.-C. Lee, Y.-F. Lo, J.-M. Wu, and M.-H. Hsieh, “Characterizing first arrival position channels: Noise distribution and capacity analysis,” *IEEE Transactions on Communications*, vol. 72, no. 7, pp. 4010–4025, Jul. 2024.
- [18] C. Yin and C. Wang, “Hitting time and place of Brownian motion with drift,” *The Open Statistics and Probability Journal*, vol. 1, pp. 38–42, 2009.